

DOI: <https://dx.doi.org/10.21123/bsj.2022.7055>

## Recent advances in the Biosynthesis of Zirconium Oxide Nanoparticles and their Biological Applications

*Salam S Alsharari*<sup>1\*</sup> 

*Muneefah A. Alenezi*<sup>2</sup>  
*Mohammed Soliman*<sup>4</sup>

*Mona S. Al Tami*<sup>3</sup>

<sup>1</sup>Biology Department, College of Science, Jouf University, P.O. Box 72341, Sakaka, Saudi Arabia

<sup>2</sup>Biology Department, College of Science, University of Tabuk, Tabuk 71491, Saudi Arabia.

<sup>3</sup>Department of Biology, College of Science, Qassim University, Qassim 51452, Saudi Arabia.

<sup>4</sup>National Plan for Science, Technology and Innovation, King Saud University, Riyadh, Saudi Arabia.

\*Corresponding author: [sssharary@ju.edu.sa](mailto:sssharary@ju.edu.sa)

E-mail addresses: [makalenezi@ut.edu.sa](mailto:makalenezi@ut.edu.sa), [tamie@qu.edu.sa](mailto:tamie@qu.edu.sa), [mesoliman@ksu.edu.sa](mailto:mesoliman@ksu.edu.sa)

Received 15/2/2022, Revised 4/4/2022, Accepted 5/4/2022, Published Online First 20/7/2022,  
Published 1/2/2023



This work is licensed under a [Creative Commons Attribution 4.0 International License](https://creativecommons.org/licenses/by/4.0/).

### Abstract:

A critical milestone in nano-biotechnology is establishing reliable and ecological friendly methods for fabricating metal oxide NPs. Because of their great biodegradable, electrical, mechanical, and optical qualities, zirconia NPs ( $ZrO_2$ NPs) attract much interest among all zirconia NPs ( $ZrO_2$ NPs). Zirconium oxide ( $ZrO_2$ ) has piqued the interest of researchers throughout the world, particularly since the development of methods for the manufacture of nano-sized particles. An extensive study into the creation of nanoparticles utilizing various synthetic techniques and their potential uses has been stimulated by their high luminous efficiency, wide bandgap, and high exciton binding energy. Zirconium dioxide nanoparticles may be used as antimicrobial and anticancer agents in food packaging. In response to the growing interest in nano  $ZrO_2$ , researchers invented and developed methods for synthesizing nanoparticles.  $ZrO_2$  nanocomposites with various morphologies have recently been created using biological (green chemistry) methods. Microbes and plants both contribute to the production of zirconia in the laboratory. Capping and stabilizing agents are provided by the biomolecules found in plant extracts, whereas microorganisms provide enzymes as capping and stabilizing agents (intracellular or extracellular). It is possible to analyze the nanoparticles produced using a variety of analytical approaches, including ultraviolet-visible spectroscopy, X-ray diffraction (XRD), transmission electron microscopy (TEM), and Fourier transform infrared spectroscopy (FT-IR). When applied to bacteria (both Gram-positive and Gram-negative) and fungi,  $ZrO_2$ NPs show promising antibacterial capabilities. Normal and malignant cells are sensitive to  $ZrO_2$  nanoparticles, which can be explained by the generation of reactive oxygen (ROS). This work discusses and describes many ways of producing  $ZrO_2$  nanoparticles, their properties, and various application possibilities.

**Keywords:** Applications, Characterization, Green synthesis, Nanotechnology,  $ZrO_2$ NPs.

### Introduction:

Nanotechnology deals with structures that range as small as 1-100nm<sup>1</sup>. Nanomaterials have different physical, chemical, and structural properties compared to their bigger counterparts. The nanomaterials' remarkable electrical, magnetic, and optical properties and surface activity are due to their nanoscale size and shape. When reduced to nanomaterials, ordinary materials exhibited extraordinary properties with regards to electrical conductivity, chemical reactivity, remarkable strength, super-paramagnetic behaviour, and other

characteristics that they do not possess at the macro or micro scale<sup>2</sup>. Compared to bulk materials, nanoparticles exhibit distinct or better size, dispersion, and shape characteristics. The quantum effect influences nanomaterial's chemical reactivity, surface heterogeneity (e.g., capping, coating), mechanical, optical, electrical and even magnetic properties. Other associated features, such as antibacterial activity, are influenced by the material's specific surface heterogeneity and area. Due to the wide variety of materials that can be

used to make nanoparticles, they are divided into four categories: 1) metallic nanoparticles (such as gold and silver), 2) metal oxides (such as VO, aluminium oxide, zinc oxide, and zinc chloride), 3) semiconductor nanoparticles (such as zinc sulphide, cadmium sulphide, and cadmium sulphide), 4) carbon nanoparticles<sup>3</sup>.

### Zirconium oxide (ZrO<sub>2</sub>) nanoparticles:

Zirconium oxide is one of the most intriguing and promising metallic nanomaterials currently available (ZrO<sub>2</sub>). In addition to being referred to as “ceramic steel”, zirconium (<sup>40</sup>Zr) is a transitional metal element with the electrical configuration [Kr] 4d<sup>2</sup>5s<sup>2</sup>. It was given this name in honour of the mineral zircon, the primary zirconium source. Naturally, it does not exist in pure form and can only be discovered in large quantities when combined. It may also be found as free oxide zirconia (ZrO<sub>2</sub>) in the mineral baddeleyite, zirconium oxide. Minerals in their natural state include a significant quantity of impurities, either elemental or radioactive. So, they cannot serve as the primary source for biomedical research purposes<sup>4</sup>. According to the researchers, these pure powdered forms may one day be utilized in biological applications. It has been widely established that ZrO<sub>2</sub> crystals may exhibit three different crystallographic symmetry types: monoclinic (m), tetragonal (t), and cubic (c) symmetry as seen in Fig.1. The temperature and pressure used to modify the crystallographic patterns of pure zirconia are the only variables that can be controlled. The monoclinic polymorph (m), the most stable form under ordinary circumstances, is stable up to 1170 °C. This type of deposit is most commonly seen in all-natural deposits. When the temperature is raised to 1170 °C, the monoclinic structure transforms into the tetragonal (t) polymorph, which has a small contraction of ~4–5% in total volume. At extremely high temperatures, the tetragonal form shrinks even more in volume until it eventually transforms into the least helpful cubic (c) symmetry at 2370°C<sup>5</sup>.

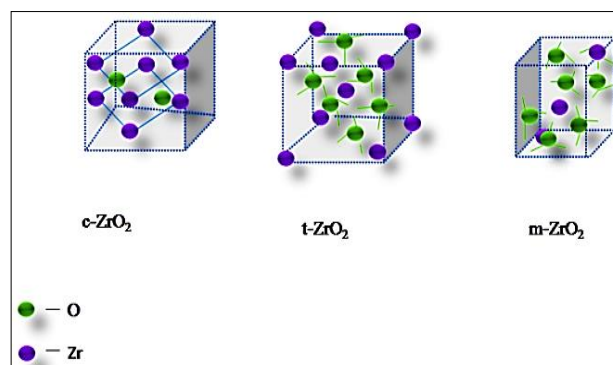


**Figure 1. Different phases of zirconia.**

In general, volume shrinkage is less prevalent in ceramics as they are heated to higher temperatures; as a result, the unusual features of zirconia enabled scientists to discover its wide range of biological uses. Furthermore, it is discovered that certain lattice modifications are reversible—cooling results in the reversion of tetragonal or cubic symmetry to the monoclinic state. The tetragonal to monoclinic transition begins at about 950 °C with a significant increase in volume (~4–5%), resulting in a much stiffer and harder lattice<sup>5</sup>. It has a natural colour, toughness, strength, corrosion resistance, chemical stability, etc. Zirconia is a wide bandgap p-type semiconductor with a bandgap 3.25 to 5.1 eV depending on the preparation method. Zirconia nanoparticles are available in nanofluids, nanocrystals, and nanodots. Zirconium oxide is also known as zirconia, zirconic anhydride, and zircol<sup>5</sup>.

In recent years, metal and metal oxide nanoparticles have been of much interest due to their varied applications, especially their antimicrobial properties<sup>6</sup>. ZrO<sub>2</sub>NPs have sparked a lot of study attention amongst transition metal oxide nanoparticles (NPs) because of their inimitable electrical, heat, catalyst, sensing, optical, mechanical, and compatible biological capabilities<sup>7</sup>. Nevertheless, due to the acidic and basic composition, ZrO<sub>2</sub>NPs is a well-familiar p-type semiconductor with piezoelectric properties<sup>8</sup>. As a result, ZrO<sub>2</sub>NPs are commonly employed in various purposes such as implant materials, dental implants, photocatalyst, refractory, fuel-based cells, gas sensors, solar cells, tissue engineering, biomarkers, drug delivery, theragnostic, water treatment, bio-conjugation and agriculture<sup>9</sup> etc. Furthermore, owing to their inimitable physiochemical characteristics, ZrO<sub>2</sub>NPs have antifungal, antioxidant and carcinogenic effects. Zirconia (ZrO<sub>2</sub>) is a material of importance with high chemical stability, strength, and corrosion resistance<sup>10</sup>. The applications of ZrO<sub>2</sub>nanoparticles are presented in Fig. 2.

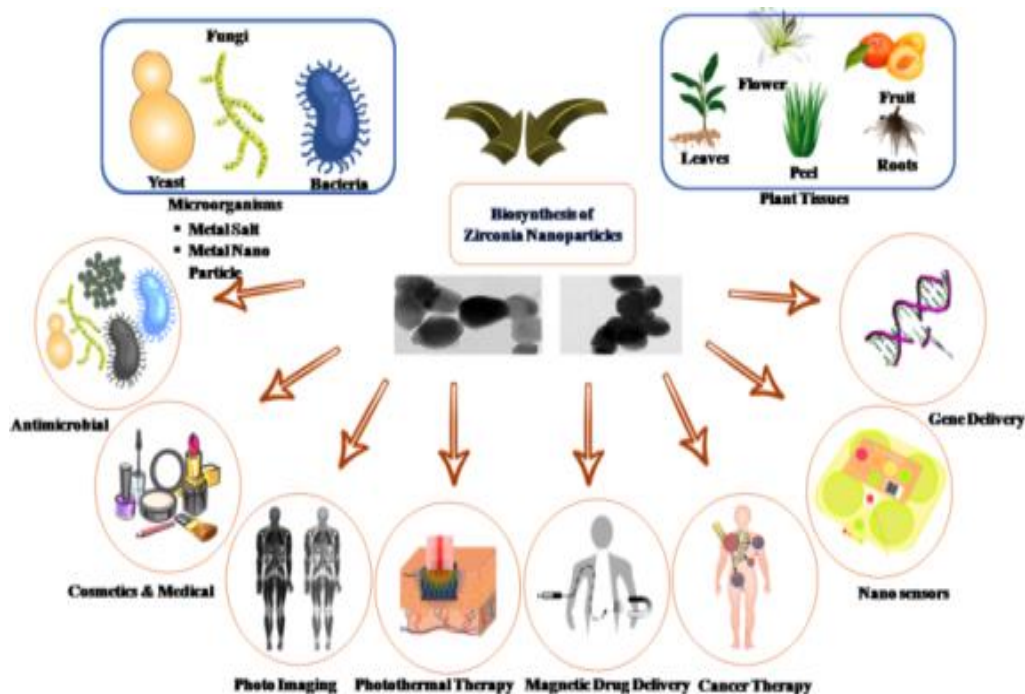


Figure 2. The applications of  $ZrO_2$  nanoparticles.

### Synthesis of $ZrO_2$ Nanoparticles:

Zirconia was synthesized through various methods like ball-mill assisted, ultrasonic abetted, sol-gel, electrical arc-based discharge<sup>11</sup>, precipitation<sup>12</sup>, hydrothermal<sup>13</sup>, heat plasma path<sup>14</sup>, solvothermal<sup>15</sup>, explosive emulsion<sup>16</sup>, microwave-assisted<sup>17</sup>, and electrochemical deposition<sup>18</sup>. However, these artificial approaches necessitate high temperature and pressures, a more

extended reaction period, expensive and hazardous chemical forerunners, and the use of specialized tools for investigational work, all of which have a detrimental environmental impact<sup>19</sup>. It is preferable to chemically manufacture nanomaterials to employ biological techniques, such as enzymatic processes, to synthesize small particles like nanoparticles. Fig. 3 illustrates the various ways used to synthesize  $ZrO_2$  nanoparticles.

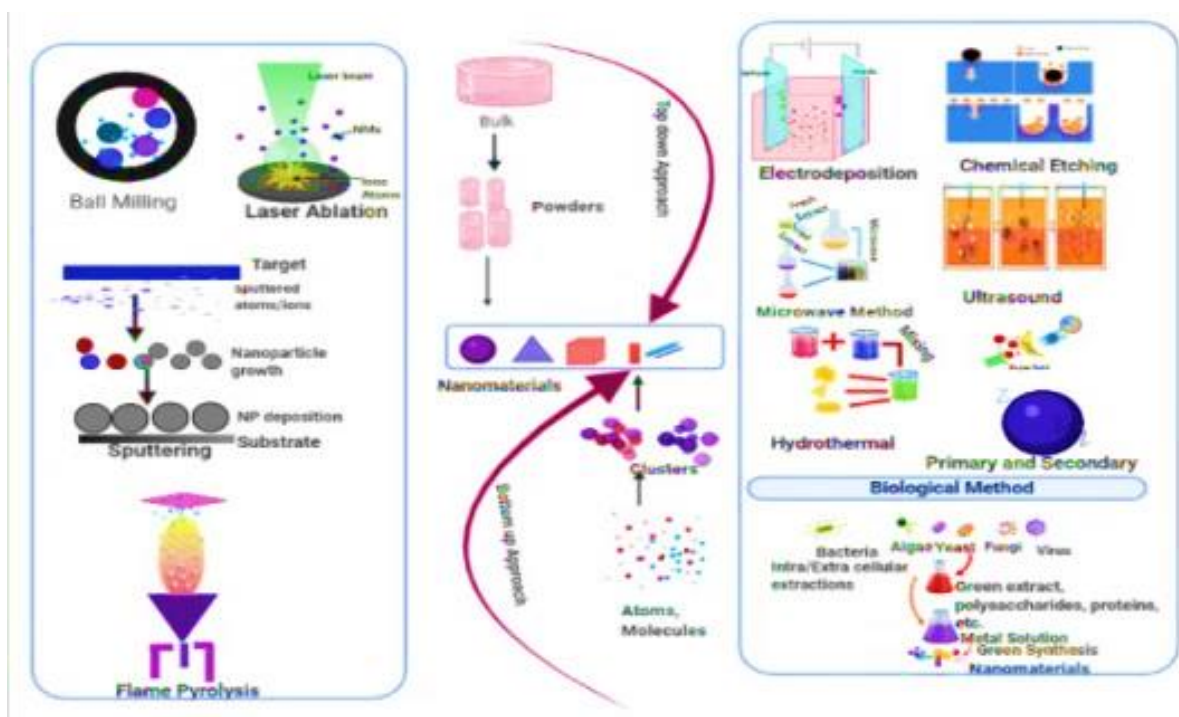


Figure 3. Synthesis of  $ZrO_2$  nanoparticles using a variety of techniques.

### Possible mechanism of formation of $ZrO_2$ NPs by using plants:

The underlying molecular pathways that contribute to the creation of NPs, on the other hand, are still poorly understood. Multiple studies have demonstrated that various metabolites can reduce and stabilize metallic NPs and avoid agglomeration and aggregation of new metallic NPs in nonhazardous ways<sup>20</sup>. In general, phenolic chemicals inactivate ions through a process known as chelation<sup>21</sup>. The chelating characteristics of phenolic aromatic rings are likely due to their high nucleophilic natures<sup>22</sup>. The most significant functional groups in metal ion reduction are carbonyl, hydroxyl, amino, and methoxide. These groups connect to the metal ions by electrostatic contact, causing them to be reduced<sup>23</sup>, and the reduction of metal ions in the result. Natural sources respond to heavy metal stress by synthesizing phyto-chelations or metal-chelating peptides<sup>24</sup>. Metal ions are chemically immobilized and

subsequently reduced, sintered, and smelted to produce nanoparticles (NPs). Metal ion concentration and ion penetration site affect the size and shape of nanoparticles<sup>25</sup>. It is possible to manipulate the shape, dispersion, and yield of these biosynthetic NPs by altering the reaction conditions<sup>26</sup>. In the absence of a protective barrier, high polyphenol levels inhibited coalescence and aggregate formation. Metal nanoparticle bio-reduction using plant extracts involves three steps. In the first step, metal ions are reduced and nucleated. Second, small adjacent NPs combine to produce larger particles, increasing their thermodynamic stability and finally, the termination phase shapes the NPs<sup>27</sup>. These are then centrifuged with the metal ion precipitates and rinsed with a suitable solvent to remove any leftover impurities before reuse. Fig. 4 presents the possible mechanism of the formation of  $ZrO_2$ NPs using plant extract.

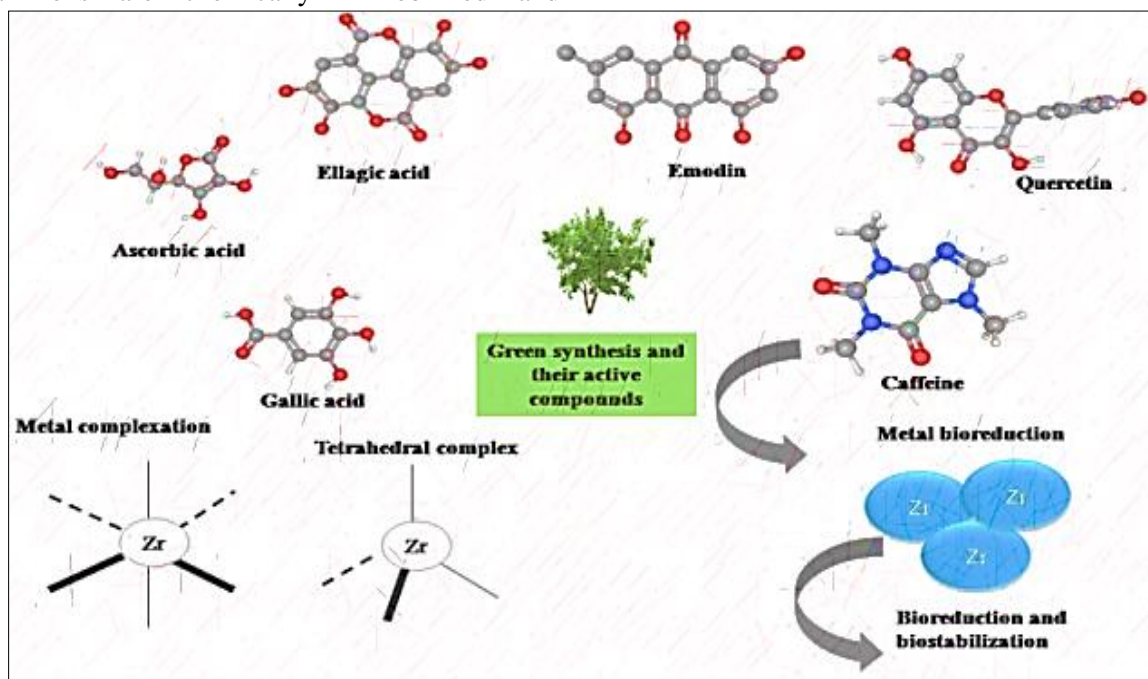


Figure 4. Possible mechanism of formation of  $ZrO_2$ NPs using plant extract.

### Green synthesis of $ZrO_2$ NPs:

Much research shows that biological production of metallic and metal oxide nanoparticles is more eco-friendly than chemical or physical approaches. Let's consider the biological synthesis process, it employs renewable resources, better solvents and auxiliaries, and produces compounds that are safer to handle than traditional chemical synthesis methods. Plant extracts are prepared by crushing or boiling plant components in appropriate solvents at specific temperatures to generate a concentrated extract. Because of the phytochemicals in plant extracts, zirconia synthesis

is made easier by acting as both a reducing and capping agent. The zirconia solution is centrifuged at higher rpm to separate the nanoparticles from the rest of the solution. After that, the pieces are completely rinsed, and the resulting solution is dried. In this process, the solution is subjected to a thermal treatment, and the  $ZrO_2$  powder is produced. Much research shows that biological production of metallic and metal oxide nanoparticles is more eco-friendly than chemical or physical approaches. The phytochemicals present in the plants is presented in Fig. 5.

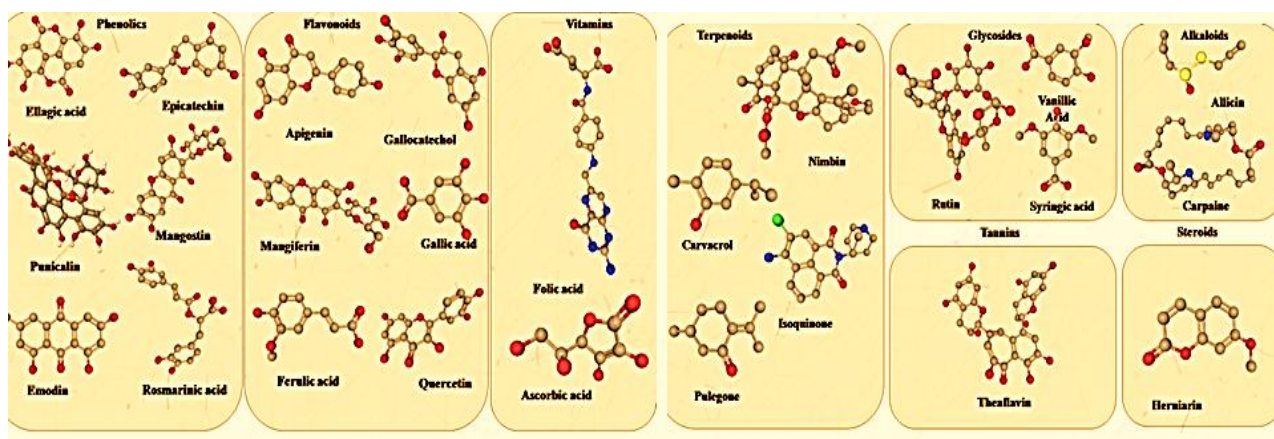


Figure 5. Phytochemicals present in the plants.

Another characteristic of agglomeration is that the time interval between the heat treatment and the creation of clusters might have an impact on their formation<sup>28</sup>. Extended agglomerates and particle development were seen by Dhadapani et al. when the period of the heat treatment at 50°C was increased from 30 to 90 minutes, according to their findings<sup>29</sup>. All of these observations are consistent with the results obtained from other chemical synthesis processes. The lengthening of the time required for nucleation resulted in bigger particles of ZrO<sub>2</sub>. It is also known that the pH conditions used during the synthesis process may drastically alter the particle size and shape of metals and metal oxides, which will, in turn, change the characteristics of the nanomaterials produced by the process. The pH of the solutions of the biological extracts used in the green production of ZrO<sub>2</sub>NPs is not considered in much of the previous research.

#### Synthesis of ZrO<sub>2</sub>NPs using plants:

The use of *Acalypha Indica* leaves for Zirconia nanoparticle formation was noticed, where ZrOCl<sub>2</sub>.8H<sub>2</sub>O was used as the precursor<sup>30</sup>. In this work, FTIR results showed a fundamental part in showing the significant functional groups in the ZrO<sub>2</sub>NPs. The SEM and XRD studies showed that the average size of the NPs was recognized as 20-100 nm with cube-shaped ZrO<sub>2</sub>NPs. Gowri et al.<sup>31</sup> synthesized flake like nanostructures of ZrO<sub>2</sub> using zirconium oxychloride (0.4M) and aqueous extract of *Nyctanthes arbortristis*. In this study, to evaluate the optimum calcination temperature to generate ZrO<sub>2</sub> crystalline NPs with a characteristic phase, the as-synthesized specimen was then imperilled to calcinations in a muffle furnace at 300°C and 500°C for 3 hrs. From this work, the authors stated that the ZrO<sub>2</sub>NPs (43 nm) at 300 °C exhibit lesser size and adequate crystallinity with tetragonal phase structure. Two bacterial species, Gram +ve (*S. aureus*) and Gram -ve (*E. coli*), were

used to study the antibacterial activity. However, *E. coli* bacteria hold more inhibition (30mm) when compared to *S. aureus* when treated with ZrO<sub>2</sub>NPs synthesis at 300°C on cotton fabric.

Kanda et al.<sup>32</sup> synthesized ZrO<sub>2</sub>NPs utilizing *Thespesia populnea* plant extract to perform on cotton gauze fabric for the antibacterial action of nano-zirconia. In this study, to prepare NPs, zirconyl chloride of 1 mM that is 80 mL, is introduced to the extract of *T. populnea* by 20 mL. A reaction medium was agitated for a period of 2 hrs at an of 80 °C temperature as well a reaction mixture leaves for a full night for NPs creation without shaking. After that, sediment is vacuum dried in an oven at a temperature of 200 °C for 1 to 2 hrs to attain ZrO<sub>2</sub>NPs. From UV-Vis spectroscopy, the stronger peak formed by ZrO<sub>2</sub>NPs after 200nm designated that formation of ZrO<sub>2</sub>NPs. XRD and TEM analysis, the synthesized NPs were found 10 nm. In the functional group analysis, the stronger bands among 500 and 400 cm<sup>-1</sup> were accredited to a stretch of -OH group representing stretch and a bend of H<sub>2</sub>O absorbing through ZrO<sub>2</sub>NPs. The absorbing peaks at 3220.28, 2921.01 and 1608.02 to 698.94 cm<sup>-1</sup> are due to its asymmetrical vibrational stretch formed through the -OH group of absorbing H<sub>2</sub>O. The maximum zone of inhibition attained towards *E. coli*, *S. aureus*, *B. subtilis*, and *P. aeruginosa* tested by well diffusion method as 26, 25, 11 and 8 mm, respectively.

Veronika et al.<sup>33</sup> developed green methods for producing zirconium oxide-gold (ZrO<sub>2</sub>-Au) core-shell nanocomposites using *Equisetum arvense* extract via bio-reduction method. From UV-Vis results, the SPR peaks for the Au/ZrO<sub>2</sub> bi-phasic system centre at 539 nm, but no peak was observed for ZrO<sub>2</sub>NPs. From STEM analysis, the formed AuNPs appeared as spherical and triangular-shaped; the dominant sample shape was spherical rather than triangular. While spherical Au NPs ranged

from 6–44 nm with an average 24 nm diameter. The size distribution of triangular-shaped NPs ranged from 20 to 200 nm. A negative charge (-17.5mV) was observed from zeta potential results due to active phytochemicals with long-term change effects that stabilize NPs and serve as capping agents.

*Aloe vera* extract was employed as a capping and reducing agent in the biological processes used by Gowri et al.<sup>34</sup> to produce nanoparticles. In the UV-Vis spectrum, the seemed at 213 nm was blue lifted from solid ZrO<sub>2</sub> substance and distinctive for tetragonal ZrO<sub>2</sub>NPs. From SEM and AFM analysis, spherical-shaped structures by smoother and attached surfaces and weaker accretion of atoms were evidently determined homogeneously with less than 50 nm. From thermal analysis, an endothermic peak that appeared at below 150°C and 350°C might be linked to the release of surface adsorbing H<sub>2</sub>O and organic components adsorbed in the as-prepared Zr. The formed ZrO<sub>2</sub>NPs preserved fabrics exhibited larger antimicrobial action towards *E. coli* (32 mm) microbes than with *S. aureus* (23mm) bacteria with a zone of inhibition (ZOI) 32 and 23 mm, respectively.

Pragya et al.<sup>35</sup> developed a green, non-toxic and lower-cost creation of monoclinic ZrO<sub>2</sub>NPs by utilizing a green production study from a methanol-based *Helianthus annuus* seed extract as

plummeting substance. The UV-Vis spectrum is sharper and rises at 275 nm owing to its valence to conducting band shift. The zeta potential as -9.32 mV and particle size distribution of ~331 nm is used to illustrate the sustainability of NPs. Because of the transition of enol compounds into ketones, the -H atom is released, which lessens the ionization of the molecules in zirconium salt, which is beneficial. As a result, following the annealing process, it contains zirconium oxide nanoparticles since the other organic compounds are no longer present below the temperature used for the annealing process. The SEM and TEM study of ZrO<sub>2</sub>NPs displayed spherical shape-based and mean-particle size 35.45 nm. From EDX pattern of ZrO<sub>2</sub>NPs exposed the existence of Zr as 77.92 %, O as 13.89 %, and carbon as 8.28 %, a major element of the specimen. ZrO<sub>2</sub>NPs exhibited antibacterial activity when tested with Gram +ve *S. aureus* and Gram -ve microbes (*E. coli*, *P. aeruginosa*, and *K. pneumoniae*). The agar well diffusion method showed Gram-negative microbes with ZOI were 12, 13, 13.5 and 12.5 mm, respectively. ZrO<sub>2</sub>NPs might be the resource that generated ROS, which resulted in the suppression of strains containing gram-negative bacteria. These ZrO<sub>2</sub>NPs were shown to be closely related to the bacterium cell wall's lowest point. The possible mechanism of modified antibacterial activity of zirconia was presented in Fig. 6.

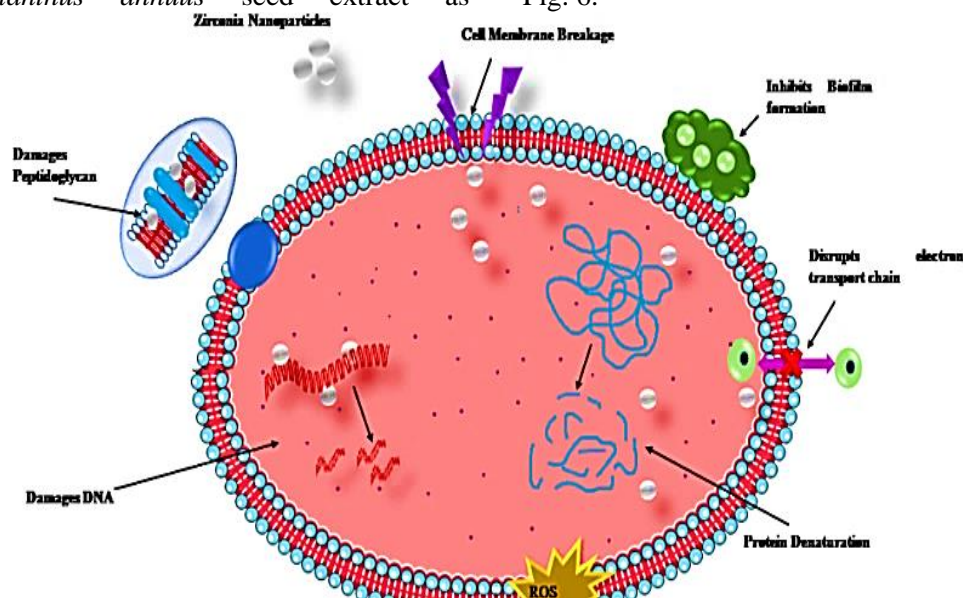


Figure 6. Possible mechanism of modified antibacterial activity of zirconia<sup>35</sup>.

Annu et al.<sup>36</sup> prepared ZrO<sub>2</sub>NPs through bio-based procedure utilizing *Moringa oleifera* leaf extract. UV-Vis spectrum showed an absorption band at 293 nm that authorizes the blend of tetragonal ZrO<sub>2</sub>NPs. A spherical-shaped smooth surface with particles size below 10 nm was observed from SEM and XRD analysis. The

synthesis ZrO<sub>2</sub>NPs unveiled 69.4% suppressing action against the free radicals. ZrO<sub>2</sub>NPs formed by *Moringa oleifera* showed antimicrobial action towards Gram -ve and +ve microbes like *E. coli*, *P. aeruginosa*, and *B. subtilis*. This is due to the fact that the negatively charged cell wall of Gram -ve bacteria is attracted to the positively charged

zirconium ions contained within the nanoparticles, resulting in the cell death of the organism in the process. In another work, Isaacfranklin et al.<sup>37</sup> developed a procedure for the creation of ZrO<sub>2</sub> nanorods by nanorods, which included the use of 10 mL of *Nephelium lappaceum* L. fruit peel and hydrothermal treatment to produce the nanorods. From XPS analysis, a protuberant band and a shoulder band are positioned at 183 and 185 eV, resembling Zr3d<sub>5/2</sub> and Zr3d<sub>3/2</sub>, and the O1s spectra attained in the 530–531 eV ranging that was accountable for the Zr–O/O–H elements. The typical monoclinic structural peaks were caused by Raman peaks detected at 180, 192, and 475 cm<sup>-1</sup>. The maximum suggests cubic zirconia production at 475 cm<sup>-1</sup>. The prepared ZrO<sub>2</sub> nanorods were shown antitumor efficiency towards human breast tumour cells (MCF-7) and inhibiting the tumour growth in a dosage-based way at a half-maximal inhibition level of 55.32 µg mL<sup>-1</sup>.

Kumar et al.<sup>38</sup> prepared a chitosan-based ZrO<sub>2</sub>NPs blend of Zr NPs utilizing an aqueous *Aloe vera* extract and characterized by UV-Vis, TEM, EDAX, XRD and FT-IR study. The UV–vis absorption peak of the produced Zr NPs was 420 nm. The generation of polydispersed NPs varying in size from 18 nm to 42 nm was revealed by TEM. SAED and XRD examination revealed that the Zr crystallites were fcc (facial centred cubic). Zr was found to be an essential component of synthesized NPs, according to EDAX analysis. At pH 7.0, fluoride adsorption on the CNZr composite performed well, with 99 % of fluoride retained. Anderson et al.<sup>39</sup> used *Euclea natalensis* extract to synthesize zirconia NPs. During the synthesis of NPs in this experiment, the extract concentration was changed from 50 to 75 to 100g/L for precursor doses of 0.01, 0.02, and 0.03 mol/L, respectively. The tautomeric transition of enol compounds into keto compounds, for example, releases the reactive hydrogen atom, lowering the zirconium ions in the molecule. The calcination produced zirconia nanoparticles since the organic matter created during the process is destroyed at the temperatures used. XRD shows monoclinic and tetragonal phases in zirconia with crystallite diameters of about 5.25 nm. The particles were spherical and had a relatively small average diameter of 5.90 to 8.54 nm. Furthermore, the NPs have executed the tetracycline 30.45 (mg/g) adsorption.

Siripreddy et al.<sup>40</sup> prepared ZrO<sub>2</sub>NPs using *Eucalyptus globulus* (*E. globulus*) extract with spherical by the size varying from 9–11nm and with higher zeta potential -45.5 mV. The identified cytotoxic action of ZrO<sub>2</sub>NPs was caused through ROS. Furthermore, green produced ZrO<sub>2</sub>NPs had

stronger antioxidant capacity, neutralizing as 85.6 % of free radicals released through the DPPH. The computed IC<sub>50</sub> for non-cancerous Vero cells are 228 g/mL, indicating that ZrO<sub>2</sub>NPs are less harmful to normal cells. Gurushantha et al.<sup>41</sup> produced cubic ZrO<sub>2</sub>: Fe<sup>3+</sup> (0.5–4 mol%) NPs using *Phyllanthusacidus* as a reducing agent. Under UV and sunlight irradiation, Fe<sup>3+</sup> on ZrO<sub>2</sub> matrices influenced photocatalytic depletion of AO7. Shinde et al.<sup>42</sup> carried out an experiment on the Biosynthesis of ZrO<sub>2</sub>NPs by means of *Ficus benghalensis* extract as capping material for the initial time. The produced ZrO<sub>2</sub>NPs have a spherical shape with a size of 15 nm, which is in good accord with the XRD data. The quantum variation causes a drop of bulk ZrO<sub>2</sub> in a bandgap from 5.3 to 4.9 eV. BET findings indicate as-synthesized ZrO<sub>2</sub>NPs are a larger (88 m<sup>2</sup>/g) specific surface area. In addition, ZrO<sub>2</sub>catalyst decolorizes the methylene blue, and methyl orange photodegraded nearly 91 and 69 % in 240 minutes. Sai Saraswathi et al.<sup>43</sup> synthesized of ZrO<sub>2</sub>NPs from *Lagerstroemia speciosa* leaf. The highest absorption spectrum of processed ZrO<sub>2</sub>NPs from a leaf of *L. speciosa* displayed a peak at 354 nm. The EDX pattern indicates maximum emanation at 1 keV that was the binding energy of Zr (70.4 %), and 0.5 keV have binding energy for O<sub>2</sub>(24.11 %) and enduring creates carbon-based constituent. A photocatalyst action of ZrO<sub>2</sub>NPs was considered for azo dye through revealing to sunlight with 94.58 %. The number of deaths cells rose as the quantity of ZrO<sub>2</sub>NPs doubled. Cells shrank at 500 g/mL, and almost 30–40 % of cells exhibited blebbing (tiny protuberances of the membrane). In the ZrO<sub>2</sub>NPs treated cells, apoptosis bodies were found. Nabil et al.<sup>44</sup> synthesized ZrO<sub>2</sub>NPs using leaf extract of *Wrightia tinctoria*. An emission spectrum causes an emission of the ZrO<sub>2</sub>NPs at 360 nm, which can be seen in the PL spectrum. An average ZP value of -21.17 eV indicated a capping particle on the surfaces of produced ZrO<sub>2</sub>NPs was primarily made up of negative charges. For 120 minutes, the biologically synthesized ZrO<sub>2</sub>NPs degraded RY 160 dye by 94 %. At a dose of 10 µg/ml, the aqueous *W. tinctoria* extract showed the maximum inhibitory zone towards *E. coli* (12 ± 0.2), *S. aureus* (10 ± 0.1), *P. aeruginosa* (9 ± 0.4), and *B. subtilis* (7 ± 0.3). Biosynthesized ZrO<sub>2</sub>NPs produced by *W. tinctoria* extract demonstrated excellent antibacterial effectiveness against all tested microbes when compared to leaf extract at 10 g/ml. Inhibition zones were observed for *E. coli*, *S. aureus*, *P. aeruginosa*, and *B. subtilis*, which had 22.5 mm, 21.5mm, 21.5mm and 20mm, respectively. The nanoparticle's tiny spherical shape and crystallite size may be to blame for their

enhanced antibacterial properties. Vanadium oxide ( $V_2O_5$ ) or  $ZrO_2$  NC were made by Parsa et al.<sup>45</sup> utilizing *Daphne alpine* (*D. alpine*) leaves extract in a green method. The pore space and surface area were investigated utilizing Brunauer-Emmett-Teller (BET) techniques for the  $N_2$  adsorption-desorption process, and SBET was determined to be  $214 \text{ m}^2/\text{g}$ . Diffuse reflectance spectroscopy (DRS) was used to investigate the optical property, and the absorption edge was discovered to be 3.93 eV. Around  $3499 \text{ cm}^{-1}$ , the stretching vibration of the -OH group was noticed. The -C-H bending characteristic peaks about  $3000$  and  $2942 \text{ cm}^{-1}$ , while the bands at  $1725 \text{ cm}^{-1}$  could be attributable to the carbonyl group (C=O) of the ester and carboxylic acid. The -NO bend mode and carbonyl stretch are responsible for the peaks at  $1433$  and  $1220 \text{ cm}^{-1}$ , respectively. When methyl orange and picloram were used as photocatalysts, the photocatalytic efficacy of  $V_2O_5/ZrO_2$  NC was tested, and 76.94 % and 86 % were destroyed in 75 minutes, respectively.

Annu et al.<sup>46</sup> prepared  $ZrO_2$ NPs utilizing the pericarp extract of *Sapindus mukorossi* as a prevailing capping and reducing agent. The particle size was 5–10 nm that, was in accord with the tetragonal stage. Distinct peaks were observed only in EDX spectrum to Zr, and the broad -OH stretching contributes to the large and prominent band at  $3180 \text{ cm}^{-1}$ . The acute, tight spike at  $1655 \text{ cm}^{-1}$  was attributable to the processed specimen's bend vibration adsorbed  $H_2O$  structures. The distinctive tetragonal Zr-O-Zr vibration that was predominantly amplified through the calcination method considerably contributes to the peak occurrence in the region of  $500-700 \text{ cm}^{-1}$ . In batch trials, the adsorptive capabilities of produced NPs for methylene blue (MB) dye were investigated as a function of pH, dose, initial adsorbate level, and time. With an adsorptive capacity of  $23.26 \text{ mg/g}$ , 94 % removal performance was found, which aligned well with the nonlinear Langmuir isotherm.

Vennila et al.<sup>47</sup> produced  $ZrO_2$ NPs that used a methanol-based extract of *Glorisa superba* tuber powder. The produced NPs were analyzed using XRD, SEM, and EDX techniques and a solar cell simulator approach to investigate the natural dye-sensitized solar cell activity of  $ZrO_2$ NPs. The photocurrent in the DSSC's photoanode, which accumulates of analyzing stage ZnO/TiO<sub>2</sub>NPs with opuntia dye on the FTO substrate, was studied. Renuka et al.<sup>48</sup> generated  $ZrO_2$  doped with Mg hollow-based microspheres with a 0.1-5 mol% using a simple, environmentally benign, low-cost phytomediated burning technique. The peak related to (-111), (002), and (111) planes marginally migrated to lesser  $2\theta$  angle side when  $Mg^{2+}$  level

increased from 0.1 to 2 mol % in this investigation; however, these planes moved slightly greater  $2\theta$  angle side as  $Mg^{2+}$  concentration increased from 3 to 5 mol %. The bands confirmed the monoclinic phases of  $ZrO_2$  at  $100, 179, 192, 222, 306, 340, 380, 470, 510,$  and  $540 \text{ cm}^{-1}$ . The existence of tetragonal and monoclinic phases in  $ZrO_2: Mg$  4 mol %NPs was confirmed by Raman bandings at  $147$  and  $260 \text{ cm}^{-1}$ . Under UV light, the photocatalytic capabilities of photocatalysts are assessed for the destruction of rhodamine B. The photocatalytic performance of 2 mol % Mg enriched  $ZrO_2$  was good, with a dissolution rate of 93 %. Compared to pure  $ZrO_2$ , 2 mol % Mg-doped  $ZrO_2$  showed the highest photocatalyst reaction and the largest particular surface area and pore volume. This could aid with dye loading as well as photocatalytic reactivity. Nevertheless, 2 mol % Mg-doped  $ZrO_2$  and 5 mol % Mg-doped  $ZrO_2$  have the highest surface area and pore volume but low photocatalyst activity. In another study, Sathish Kumar et al.<sup>49</sup> developed liner chains of  $ZrO_2$ NPs using *Curcuma longa* with an average size of range 41-45nm. The Tem image of  $ZrO_2$  particles was presented in Fig. 7.

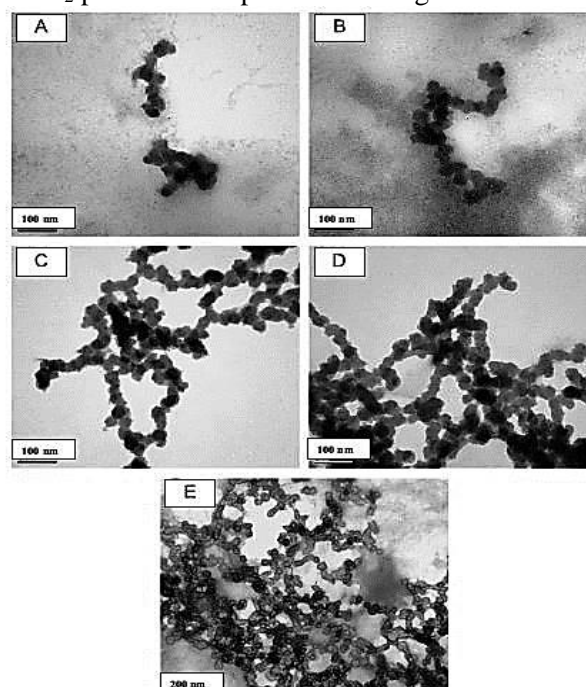


**Figure 7. TEM image of zirconia nanoparticles. Adopted with permission from ref<sup>49</sup>.**

The organized NPs evidently showed peaks that corresponded to the monoclinic  $ZrO_2$  stage at  $28.8$  (111),  $41.2$  (102),  $50.7$ (122),  $59.1$ (131), and the rhombohedral  $Zr_3O$  phase 1025) at  $53.9$  (0117). The strength of organic compound bands decreases relate to -COOH group vibrations and  $2922$  and  $2854 \text{ cm}^{-1}$  to C-H vibrations. A specimen of Zr salt to rosemary extract produced small finer particles around 12 and 17 nm, according to the findings.



The elastic modulus of PVA measured amount of Zr NPs and decreased at higher Zr NP content, as per observations. When contrasted to polymeric matrix, the specimen by 1 wt%. ZrO<sub>2</sub>-PVA had good elastic modulus. The next stage is the H-bonding amid the -OH groups on ZrO<sub>2</sub>NPs and the -OH functional group of PVA particles. The -OH group in the PVA framework may combine with the surface of ZrO<sub>2</sub>, which is used as a filler, to produce hydrogen. The nanocomposite was stabilized by hydrogen bonding, which prevented the dissociation of phase<sup>50</sup>.

Pandiyan et al.<sup>51</sup> developed CeO<sub>2</sub>@ZrO<sub>2</sub> core metal oxide (MO) NPs utilizing *Justiciaadhatoda* extract. The broad peaks at 267, 305 and 615 cm<sup>-1</sup> of ZrO<sub>2</sub> were noticed in Raman spectra CeO<sub>2</sub>@ZrO<sub>2</sub> core metal oxide NPs at a temperature of 700 °C, which was the characteristic tetragonal stage of Zr. According to the XRD results, CeO<sub>2</sub>@ZrO<sub>2</sub> core metal oxide NPs, a proportion of ceria-0.75, Zr-0.25, and two O<sub>2</sub> contents demonstrate that CeO<sub>2</sub>@ZrO<sub>2</sub> core metal oxide NPs has the formula (Ce0.75+ Zr0.25) O<sub>2</sub>. The nano stick shape of CeO<sub>2</sub>@ZrO<sub>2</sub> core metal oxide was visible in the micrographs. The CeO<sub>2</sub>@ZrO<sub>2</sub> core metal oxide MO inhibited violacein synthesis in *C. violaceum* in a violacein inhibition assay (ATCC 12472). CeO<sub>2</sub>@ZrO<sub>2</sub> gradually depletes the nutrients bacteria require development, resulting in cell death. The antimicrobial property of CeO<sub>2</sub>, ZrO<sub>2</sub>, and CeO<sub>2</sub>@ZrO<sub>2</sub> core metal oxide NPs was tested towards *S. aureus* and *E. coli* microbial infections. For both infections in the order *S. aureus* > *E. coli*, CeO<sub>2</sub>@ZrO<sub>2</sub> alone have revealed a diameter of inhibition zone *S. aureus* as 34 mm, following by *E. coli*, displayed the best and highest antimicrobial

property in the CeO<sub>2</sub>@ZrO<sub>2</sub> core metal oxide NPs as 29 mm. The antioxidant behaviour of core metal oxide has a special characteristic that requires less energy of DPPH radical by up to 89%. *S. marcescens* was used to assess the antibiofilm action of CeO<sub>2</sub>@ZrO<sub>2</sub> core metal oxide NPs. Antibiofilm features of CeO<sub>2</sub>@ZrO<sub>2</sub> core metal oxide NPs are shown in the study, and they were able to harm the multilayer, 3D biofilm structure. The CeO<sub>2</sub>@ZrO<sub>2</sub> core metal oxide NPs limit quorum sensing and govern the growth of *S. marcescent* biofilms.

Raghad et al.<sup>52</sup> green synthesis of ZrO<sub>2</sub>NPs utilizing different plant extracts: *Capsicum annum*, *Allium cepa* and *Lycopersicon esculentum*. NPs was produced by *C. annum*, their properties according to method one and method two were: average size was 100.25 nm, 86.66 nm, roughness average (Ra) 1.17 nm and 1.08 nm, Root mean square (Sq) 1.98 nm, 1.25 nm. Scherer's equation also calculated crystal's size; it was 22.029 nm and 13.069 nm, optical band gaps were 5.1 eV and 5.25 eV, and according to SEM, particles size were (<105, 100) nm, respectively. NPs produced by *A. cepa*, their properties according to method one and method two were: average size was 105.14 nm, 83.00 nm, (Ra) was 0.238 nm, and 1.09 nm, (Sq) was 0.272 nm and 1.27 nm. Crystals sizes were 11.039 nm and 21.97 nm, optical band gaps were 5.3 eV and 3.9 eV, and according to SEM, particles size were (>80, >90) nm, respectively. Zirconium NPs were confirmed for their antimicrobial efficacy towards microbial cultures of *E. coli* and *S. aureus* by well diffusion method. Plant mediated synthesis of nano zirconium particles is presented in Table 1.

**Table 1. Plant extract mediated synthesis of nano zirconium particles**

Plant extract	Characterization	Size (nm) & shape	Functional groups	Applications	Ref.
<i>Acalypha Indica</i> (20g, 200ml)	FT-IR, XRD, SEM, EDX	20-100& cubic	Zr-O-Zr asymmetric stretching, -OH stretching and bending vibration	N/A	Shanthi et al. <sup>30</sup>
<i>Nyctanthes arbor-tristis</i> (5g, 50ml)	TG/DTA, XRD, SEM, EDX, AFM and UV-Vis	150& flake-like	NA	Antibacterial	Gowri et al. <sup>31</sup>
<i>Thespesia populnea</i> (2.435 g, 20 ml)	UV-vis, XRD, TEM and FTIR	10, Spherical	O-H group of the absorbed water, C-H and C-O groups	Antibacterial	Kanda et al. <sup>32</sup>
<i>Equisetum arvense</i> (3gm,150ml)	UV-vis, STEM, DLS and zeta potential	24-40, Spherical & triangular	$\beta$ -sitosterol, campesterol, isofucoesterol, ascorbic acid; phenolic acids and polienic acids	N/A	Veronika et al. <sup>33</sup>
<i>Aloe vera</i> (50g,100ml)	TG/DTA, XRD, SEM with EDX, AFM, UV-Vis and FTIR.	50-100, Spherical	carbonyl groups, polyphenolic compounds, and -OH stretching vibrations of adsorbed water molecules	Antimicrobial & antifungal	Gowri et al. <sup>34</sup>
<i>Helianthus annuus</i>	XRD, TEM, SEM with EDX, UV-Vis, FTIR and DLS and zeta potential	35.45& spherical	C-H stretching vibrations, carboxyl group of C-O stretching, and an aliphatic amine group	Antibacterial activity	Pragya et al. <sup>35</sup>

<i>Moringa oleifera</i> (10g,100ml)	XRD, SEM- EDX, UV-Vis and FTIR	10 & spherical	-OH stretching and bending vibrations of adsorbed water, -OH stretching of phenols	Antibacterial & antioxidant activity	Annu et al. <sup>36</sup>
<i>Nephelium lappaceum</i> L. (10ml)	XPS,TEM,PL, Raman and FTIR	50& rod	O–H bending and stretching vibrations	Anticancer activity	Isacfranklin et al. <sup>37</sup>
<i>Alovera</i> (5g,20mL)	UV-Vis, TEM, EDAX, XRD and FT-IR	18–42 & spherical	O-H (of alcohol) ,CO and N H group, alkynes, alkenes and nitriles	Adsorption of fluoride	Kumar et al. <sup>38</sup>
<i>Euclea natalensis</i> (50, 75, and 100g/l)	XRD, FTIR and TEM	5.90–8.54 & spherical	stretching vibrations of the –OH group, –OH groups present in these biomolecules, such as quercetin	Adsorption of tetracylin	Anderson et al. <sup>39</sup>
<i>Eucalyptus globules</i> (10g/100ml)	UV-Visible and DRS, XRD, FTIR, TEM, SAED, SEM-EDX, DLS and fluorescence spectroscopy	9-11& Spherical	Ellagic acid, gallic acid, caffeic acid, chlorogenicacid, methyl gallate, glycosides, and phenolic compounds	Antioxidant & anticancer activity	Siripireddy et al. <sup>40</sup>
<i>Phyllanthusacidus</i>	UV-Vis, XRD, FTIR, HRTEM-EDX, SEM and PL spectroscopy	4.5 to 5.8 spherical	-OH bending and stretching of water on the surface of ZrO <sub>2</sub> , -OH of phenols	Catalytic activity	Gurushantha et al. <sup>41</sup>
<i>Ficus benghalensis</i> (5g/100ml)	UV-Vis, DRS, XRD, FT-IR, HR-TEM, FT- Raman and BET surfacearea	10– 18&spherical	C–H stretching, C=O of stretching and O–H stretching vibration	Catalytic activity	Shinde et al. <sup>42</sup>
<i>Lagerstroemia speciosa</i> (15g/100ml)	UV-vis FT-IR, X- XRD,TEM, SEM- EDX, and TGA	56.8& tetragonal	stretching of -OH bonds due to water adsorbed, the plant extract, -N-H, H-O-H bending vibrations, N-H vibrations due to the amino group and carboxylic group	Catalytic activity& anticancer activity	Sai Saraswathi et al. <sup>43</sup>
<i>Wrightia tinctoria</i> (10g/100ml)	XRD, UV-Vis, SEM- EDX, DLS, ZE, PL and FT-IR.	9.15 & spherical	O–H stretch in alcohols, phenolic and flavonoids compounds, O–H stretching of carboxylic acids and C–C stretch in aromatic compounds	Photo catalytic & antibacterial activity	Nabil et al. <sup>44</sup>
<i>Daphne alpine</i> (20g/1000ml)	DRS, XRD, TEM, SEM, TG/DTG, and FT-IR.	34-50 & spherical	-OH group, -C-H bending carbonyl group of ester and carboxylic acid, N=O bending mode and carbonyl stretching	Photo catalytic	Parsa et al. <sup>45</sup>
<i>Sapindusmukurossi</i> (5g/100ml)	UV-Vis, FTIR, XRD, SEM-EDX and HR- TEM.	5-10 & spherical	O–H stretching and bending vibration of adsorbed water moities	Adsorption	Annu et al. <sup>46</sup>
<i>Glorisa superb</i> (10g/100ml)	XRD, SEM and EAX	11.625 nm. & hexagonal	NA	Solar cell	Vennila et al. <sup>47</sup>
<i>Aloe Vera</i> (3g/20ml)	M, TEM, PL, UV-Vis, XPS, Raman, and FTIR	7-29& spherical, tetragonal and hexagonal	stretching vibration of hydroxyl group	Photo catalytic	Renuka et al. <sup>48</sup>
<i>Curcuma longa</i> 6.8 g	XRD,TEM,EDX and FTIR	41-45 & chains	Band at 818 cm <sup>-1</sup> indicated the presence of the monoclinic Zr–O–Zr	NA	Sathishkumar et al. <sup>49</sup>
<i>Rosmarinus officinalis</i>	XRD, FTIR, TGA, FESEM and tensil strength	2-30 & spherical	Vibrations of COOH and C-H vibrations	NA	Davar et al. <sup>50</sup>
<i>Justiciaadhatoda</i> 10gm/100ml	UV-Vis, DRS, XRD, FTIR,SEM-EDX, HRTEM, Raman	20-45& stick-like	Hydroxyl groups (-OH), which is an indication of alcohol and phenols	Antioxidant, antibacterial and antibiofilm	Pandiyan et al. <sup>51</sup>
<i>Capsicum annum</i> , <i>Allium cepa</i> and <i>Lycopersiconesulentum</i>	UV-Vis ,XRD, FTIR,SEM, AFM, and HRTEM	80-90& spherical	NA	antibacterial and antifungal	Raghad et al. <sup>52</sup>

### Synthesis of ZrO<sub>2</sub>NPs using bacteria:

Using microbial culture or biomass, metal and metal oxide nanoparticles can be produced in an extracellular or intracellular context. Extracellular synthesis is a process in which microorganisms manufacture enzymes and proteins that are discharged into the environment. These enzymes and proteins have decreased metal ions and stabilized particles<sup>53</sup>. In contrast to the extracellular biosynthesis pathway, the internal biosynthesis route necessitates the inclusion of a cell lysis step to release the nanoparticles from within the microbe<sup>54,55</sup>. Thus, intracellular synthesis takes longer and costs more than the extracellular production process, in which metals are reduced or chelated by proteins and enzymes outside the cell. The amino, sulfahydryl, and carboxylic groups found in the main enzymes found in biological materials attach to the metallic ions and cause them to be reduced; however, the exact production method is still not fully known<sup>56</sup>. The possible mechanism is shown in Fig. 8.

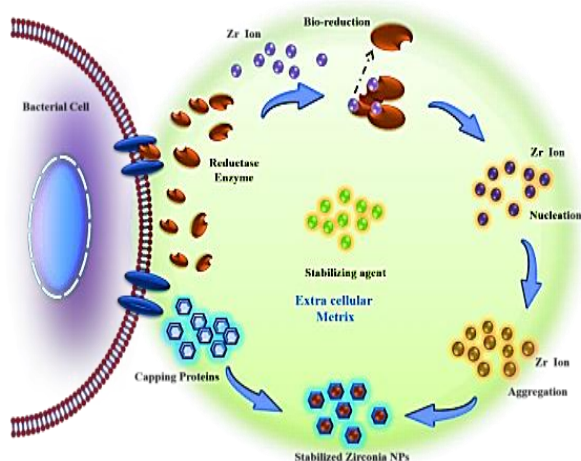


**Figure 8. Possible mechanism of formation of zirconia nanoparticles using bacteria.**

Using *Pseudomonas aeruginosa* bacteria, Banhishikha et al.<sup>57</sup> investigated the green synthesis of zirconia nanoparticles. The zirconia NPs, which had a monoclinic and tetragonal crystal structure with a crystallite size of 6.41 nm, had an average particle size of 15 nm and included zirconium and oxygen, as well as functional groups such as O–Zr–OH, Zr–O–Zr, and Zr–O–Zr bonds. There was also a monoclinic and the effectiveness of tetracycline adsorption mediated by zirconia nanoparticles was demonstrated at a pH of 6.0 and a contact period of only 15 min. TEM images show that the zirconium dioxide particles formed are spherical grains with diameters ranging from 5 nm to 25 nm and an average particle size of 15 nm. According to the findings, tetracycline

adsorption onto ZrO<sub>2</sub>NPs synthesized by the researchers followed a pseudo-second-order kinetic model. According to Temoor et al.<sup>58</sup>, ZrO<sub>2</sub> nanoparticles exhibit SPR spectra with peak ranges 240-350 nm, which is caused by the charge change from oxide species to zirconium cation (O–Zr<sup>4+</sup>). Zirconium (54.40 %), oxygen (43.49 %), silicon (0.90 %), iron (0.34 %), and aluminium (0.86 %) were all found to be present in biologically formed ZrO<sub>2</sub> nanoparticles, according to EDS spectroscopy results. The existence of the hydroxyl (O–H) group was verified by the appearance of a strong signal at 3358 cm<sup>-1</sup>. A high antifungal activity against the *P. versicolor* strain XJ27 was observed in biogenic ZrO<sub>2</sub> nanoparticles that were grown in vitro. The electron microscope pictures demonstrated that ZrO<sub>2</sub>NPs were adsorbed on the *P. versicolor* cell membrane and ruptured pathogen cells, with a continuous peak at 1637 cm<sup>-1</sup> suggesting C=C alkene stretching, which was seen in the experiments.

One pot of ZrO<sub>2</sub> nanoparticles was made at room temperature using an extremophilic *Acinetobacter* KCSII strain, according to Shanmugasundaram et al.<sup>59</sup>. Researchers found that ZrO<sub>2</sub> nanoparticles average size was 44 nm. The crystalline structure of ZrO<sub>2</sub> was discovered by the use of XRD and Raman spectra. The HRTEM and SAED pictures revealed ordered crystal lattice nanoparticles that were perfectly aligned. The zeta potential of ZrO<sub>2</sub> nanoparticles was measured to be 36.55.46 mV. In this study, the AFM was used to measure the mechanical properties of Bio-ZrO<sub>2</sub>NPs. The hardness and Young's modulus of the NPs were 9.206 2.22 GPa and 0.285 0.13 GPa, respectively. The Bio-ZrO<sub>2</sub> nanoparticles were shown to be cytocompatible, with cell viability of greater than 70% being achieved. When ZrO<sub>2</sub> nanoparticles were tested on mouse fibroblast cells, it was shown that they had no substantial cytotoxicity (L929). The highest cell viability was achieved at Bio-ZrO<sub>2</sub>NPs concentrations of 0.25 mg/mL (98.050.75 %) and 0.5 mg/mL (95.12 0.72 %), respectively (95.12 0.72 %). The dose-dependent cellular response profile of L929 cells treated with different doses of ZrO<sub>2</sub> is apparent in the Hoechst pictures taken after the cells were treated with different doses of ZrO<sub>2</sub> (Fig. 9).

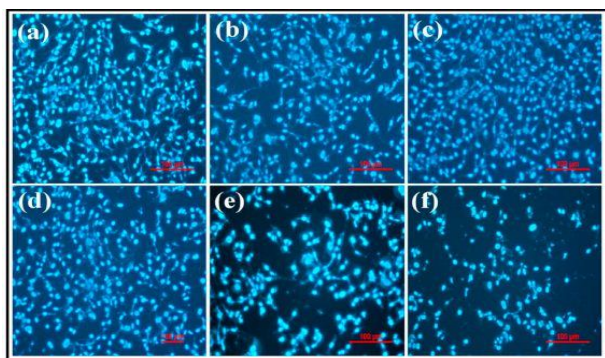


**Figure 9.** Hoechst stained images of control (a),  $ZrO_2$  at different concentrations 0.5, 0.75, 1.0, and 1.25 mg/mL (b–f) after 24 h. Adopted with permission<sup>59</sup>.

### Fungi and algae:

Similar to the reported molecular method for synthesizing metal and metal oxide nanoparticles from fungus biomass or culture, a bacterial-based green synthesis approach is also used. Green nanoparticles might be created with more efficiency using bacteria, although fungi are thought to have the best chance of success. As a result, fungus cells appear to be more resistant to changes in process conditions and variables such as pressure or flow rate as well as stirring, raising the possibility that they may be used for large-scale synthesis<sup>60,61</sup>. Heterocyclic compounds identified in proteins from fungal extracts, such as C-O-C, =C=O, C-O-R, and =C=C=, have been demonstrated to behave as NP capping ligands. Capping ligands in NPs have been shown to include functional groups such as =C=O; C-O; C-O-R; and =C=C=<sup>62</sup>.

It was established by Ahmad et al.<sup>63</sup> using AFM micrographs and SEM data that spherical NPs with a diameter of less than 100 nm could be created using this method. Using *P. notatum* PTCC 5074, *P. purpurogenome* PTCC 5212, and *P. aculeatum* PTCC 5167 as sources of colloidal zirconium nanoparticles, the zeta potential of colloidal zirconium nanoparticles was -2.2 mV, -3.87 mV, and 1.72 mV, respectively. Colloidal zirconium NPs produced with *P. purpurogenome* PTCC 5212 were efficient against Gram-negative bacteria, with MICs of 0.75 mM for *E. coli* ATCC 27853 and 0.375 mM for *P. aeruginosa* ATCC 27853, but were unsuccessful against Gram-positive *S. aureus* (ATCC 27853 and ATCC 27853, respectively). Both the supernatant and the zirconium salt solution failed to exhibit a MIC against Gram-negative or Gram-positive bacteria at a maximum concentration of 1.5 mM.

Golnaraghi-Ghomi et al.<sup>64</sup> evaluated the potential of *Penicillium notatum*, *Penicillium purpurogenum*, and *Penicillium aculeatum*

development stages to produce zirconium nanoparticles in three different growth stages. A further finding was that the electrochemical dispersive spectroscopy (EDX) of Zr-NPs displayed an absorption peak at 2.2 keV, indicating that Zr-element is present in the bio produced NPs. For PTCC 5074, PTCC 5167, and PTCC 5212, the hydrodynamic diameters of Zr-NPs at pH 7 were 22.55 nm, 66.6 nm, and 70.9 nm for the three strains studied. The correlation coefficients R<sup>2</sup> at each phase (training, validation, and test sets) were calculated using an optimal multilayer perceptron neural network to represent the experimental data, and they were found to be 0.9946, 0.9952, and 0.9997, respectively, when using an optimal multilayer perceptron neural network to represent the experimental data. An innovative approach for the production of  $ZrO_2$  nanoparticles was developed by Kavitha et al.<sup>65</sup> by utilizing the plant pathogenic fungus *Fusarium solani* as a reducing and stabilizing agent. In the HRTEM image, the spherical form of  $ZrO_2$  can be seen, with a diameter of 40-50 nm. Vipul et al.<sup>66</sup> used aqueous  $ZrF_6^{2-}$  anions to investigate the fungus *Fusarium oxysporum*. According to the authors, the hydrolysis of anionic complexes by extracellular proteins results in the simple production of nanocrystalline zirconia at room temperature. Zr–O–Zr bending vibrations can be detected by looking for an absorption band at 819  $cm^{-1}$ . At 1655 and 1544  $cm^{-1}$ , respectively, two absorption bands (amide I and II bands) are centred. The particles have a relatively uniform shape and an overall morphology that is quasi-spherical. According to the particle size histogram, particle sizes range from 3 to 11 nm, with an average of  $7.3 \pm 2.0$  nm. Under ambient settings, Uddin et al.<sup>67</sup> employed potassium hexafluorozirconate ( $K_2ZrF_6$ ) as a precursor to induce extracellular synthesis of zirconia nanoparticles in *Humicola* spp.

Algal extracts are rich in carbohydrates, proteins, minerals, polyunsaturated fatty acids, and antioxidants. Chemicals present in algae with similar carboxyl, cysteine, hydroxyl, and amine functional groups may be responsible for metal-ion reduction and capping of freshly formed nanoparticles, according to FTIR investigations<sup>68</sup>. Initial metal ions are deposited on the surface of the algal cell, which is the first step in nanoparticle creation. Depending on the kind of metal ion generated, enzymatic machinery in the cytoplasm, thylakoid membrane, and organelle membrane creates the metal ion either extracellularly or intracellularly (following metal ion intake by transmembrane protein or diffusion)<sup>69</sup>. Relying on *Sargassum wightii* (brown seaweed), Kumaresan et

al.<sup>70</sup> established a simple and ecologically acceptable combustion method for the manufacture of ZrO<sub>2</sub> nanoparticles (*S. wightii*). The structural, optical, and photoluminescence characteristics of the nanoparticles were determined. A strong absorption peak was seen at 277 nm, according to optical absorption tests. The presence of ionized oxygen vacancies in the material may be detected in PL spectra by the presence of large emission peaks at the interface of the UV and visible wavelength ranges. As seen in the TEM picture, the resultant

particles have a spherical shape and a mean particle size of 5 nm, indicating that they are relatively monodisperse. We investigated *S. wightii* extract before and after it was treated with calcinated zirconia nanoparticles for antibacterial activity against Gram-positive and Gram-negative bacteria using the agar well diffusion technique in agar wells (*Escherichia coli*, *Salmonella typhi*). Bacteria, algae, and fungi mediated the synthesis of nano zirconium particles in Table 2.

**Table 2. Bacteria, algae and fungi mediated synthesis of nano zirconia particles.**

Algae/fungi	Characterization	Size (nm) & shape	Functional groups	Applications	Ref.
<i>Penicillium</i>	FTIR, XRD, AFM, DLS and TEM	100 & spherical	O-H and C-C stretching, -OH bending mode, C=O stretching vibration of carbonyl and carboxylic group of amide I	Antibacterial	Ahmad et al. <sup>63</sup>
<i>Penicillium</i> spp.	SEM-EDX, DLS and FTIR,	100 & spherical	O-H and C-C bending, N-H bending of primary mides	NA	Golnaraghi-Ghomi et al. <sup>64</sup>
<i>Fusarium solani</i> (MTCC-2671)	FTIR, XRD, and HR-TEM	40-50&unvisual spherical	-OH stretching vibrations, amide groups, C-N stretching vibrations of aliphatic or aromatic amines	NA	Kavitha et al. <sup>65</sup>
<i>Fusarium oxysporum</i>	TEM, FTIR, SAED and XRD	3-11& quasi-spherical	Zr-O-Zr bending vibration, amide I and II bands	NA	Vipul et al. <sup>66</sup>
<i>Humicolasp</i>	UV-Vis, TEM, DLS, XPS and FTIR	13& quasi-spherical	Zr-O-Zr stretching and bending	NA	Uddin et al. <sup>67</sup>
<i>Sargassum wightii</i>	XRD, FTIR, HR-TEM, UV-vis and PL spectroscopy	5& spherical	H-bonded hydroxyl groups, stretching band of the carboxylic acid group, asymmetrical and symmetrical vibration of carboxylate ions C=O stretching at alcoholic groups	Antibacterial	Kumaresan et al. <sup>70</sup>

### Future perspectives

An eco-friendly nanotechnology is a developing approach that has applications in many areas of life and may be used to generate new, dependable, and long-lasting solutions. Thorough knowledge of the biochemical and molecular mechanisms involved in its formation is required to discover and isolate molecules involved in metal salt reduction into nanoparticles. An in-depth understanding of the distribution and mechanism of green nanoparticles' action is necessary to further biomedical uses of these particles. The most significant difficulty is the evaluation of the possible hazardous aspects of green nanoparticles and the risk management associated with their manufacturing, handling, storage, and eventual disposal. Consequently, more in-depth knowledge of metabolic processes, surface chemistry, and the chemical composition of binding agents will help researchers discover breakthrough methods that make large-scale manufacturing of binding agents possible. This green technology can provide the greatest amount of value to future generations in all

sectors of life if it can successfully battle its inherent disadvantages.

### Authors' declaration:

- Conflicts of Interest: None.
- We hereby confirm that all the Figures and Tables in the manuscript are mine ours. Besides, the Figures and images, which are not mine ours, have been given the permission for republication attached with the manuscript.
- Ethical Clearance: NA

### Authors' contributions statement:

S. S. A.: Writing and outline the study, M. A.: editing, M. A.: data analysis, M. S.: Revising. All authors contributed to data analysis, drafting, or revising the manuscript.

### References:

1. Shaimaa OH, Sumod Abdul kadhem S, Shurooq FH, Shatha MA. Antimicrobial Effect of Eco- Friendly Silver Nanoparticles Synthesis by Iraqi Date Palm (*Phoenix dactylifera*) on Gram-Negative Biofilm-Forming Bacteria. Baghdad Sci J. 2021; 18(4): 1149-1156.

2. Amal KA, Nada KA, Ruaa MA, Lamia KA. Histological and Biochemical Parameters Follow-up in Experimental rats Administrated *dexamethasone* and Treated with Green Synthesis Titanium Dioxide Nanoparticles Using (*Camillia sciences*) Extracts. *Baghdad Sci J*. 2020;17:663-669.
3. Ameen F, Dawoud T, AlNadhari S. Ecofriendly and low-cost synthesis of ZnO nanoparticles from *Acremoniumpotronii* for the photocatalytic degradation of azo dyes. *Environ Res*. 2021; 202: 111700.
4. Li K, Kou H, Rao J, Liu C, Ning C. Fabrication of enamel-like structure on polymer-infiltrated zirconia ceramics. *Dental Mater*. 2021; 37(4): e245-e255.
5. Qunbo F, Fuchi W, Huiling Z, Feng Z. Study of ZrO<sub>2</sub> phase structure and electronic properties. *Mole Simul*. 2008; 34: 1099–1103.
6. Gharpure S, Akash A, Ankamwar B. A Review on Antimicrobial Properties of Metal Nanoparticles. *J Nanosci Nanotech*. 2020; 20: 3303–3339.
7. Patil NA, Kandasubramanian B. Biological and mechanical enhancement of zirconium dioxide for medical applications. *Ceram Inter*. 2020; 46: 4041-4057.
8. Veed A, Ejub GW, Djongyang N. Study of the optoelectronic and piezoelectric properties of ZrO<sub>2</sub> doped PVDF from quantum chemistry calculations. *Chinese J Phy*. 2020; 63: 213-219.
9. Asma MA. Morphological, structural, microstructural and antibacterial features of silver-doped zirconia/hydroxyapatite for biomedical applications. *Appl Phy A*. 2021; 127: 416.
10. Elbasuney S, Gobara M, Zorany M, Maraden A, Naeem I. The significant role of stabilized colloidal ZrO<sub>2</sub> nanoparticles for corrosion protection of AA2024. *Envi Nanotech Mon Mana*. 2019; 12: 100242.
11. Karpov IV, Ushakov AV, Goncharova EA, Bachurina EP, Shaikhadinov AA. Physicochemical Properties of Zirconium Oxide Nanopowder Synthesized in Low-Pressure Arc Discharge Plasma. *Key Eng Mater*. 2020; 854: 51-56.
12. Anandan K, Rajesh K, Gayathri K, Sharma SV, Hussain SGM, Rajendran V. Effects of rare earth, transition and post transition metal ions on structural and optical properties and photocatalytic activities of zirconia (ZrO<sub>2</sub>) nanoparticles synthesized via the facile precipitation process. *Physic E*. 2020; 124: 114342.
13. Raj S, Hattori M, Ozawa M. Ag-doped ZrO<sub>2</sub> Nanoparticles Prepared by Hydrothermal Method for Efficient Diesel Soot Oxidation. *Mater Letter*. 2019; 234: 205-207.
14. Nawale AB, Kanhe NS, Bhoraskar SV, Mathe VL, Das AK. Influence of crystalline phase and defects in the ZrO<sub>2</sub> nanoparticles synthesized by thermal plasma route on its photocatalytic properties. *Mater Res Bull*. 2012; 47: 3432-3439.
15. Shaik MR, Alam M, Adil SF, Kuniyil M, Al-Warthan A, Siddiqui MRH. et al. Solvothermal Preparation and Electrochemical Characterization of Cubic ZrO<sub>2</sub> Nanoparticles/Highly Reduced Graphene (HRG) based Nanocomposites. *Mater*. 2019; 12: 711.
16. Gibot P, Quesnay F, Nicollet C, Laffont L, Schnell F, Mory J, et al. Detonation synthesis of ZrO<sub>2</sub> by means of an ammonium nitrate-based explosive emulsion. *Solid State Sci*. 2020; 108: 106405.
17. Imrana M, Rianza S, Sanaullah I, Khan U, Sabric AN, Naseem S. Microwave assisted synthesis and antimicrobial activity of Fe<sub>3</sub>O<sub>4</sub>-doped ZrO<sub>2</sub> nanoparticles. *Ceram Inter*. 2019; 45: 10106-10113.
18. Wang Y, Zhou X, Liang Z, Jin H. Characterization of Ultrasonic-Assisted Electrochemical Deposition of Ni-Co-ZrO<sub>2</sub>. *Coatings*. 2018; 8: 211.
19. Siva Sankar S, Lakshman Kumar D. Green synthesis of silver nanoparticles using *Givotia moluccana* leaf extract and evaluation of their antimicrobial activity. *Mater Lett*. 2018; 226: 47–51.
20. Singh J, Dutta T, Kim K, Rawat M, Samddar P, Kumar P. Green synthesis of metals and their oxide nanoparticles: applications for environmental remediation. *J Nanobiotech*. 2018; 16: 84.
21. Akintelu SA, Folorunso AS. A Review on Green Synthesis of Zinc Oxide Nanoparticles Using Plant Extracts and Its Biomedical Applications. *Bio Nano Sci*. 2020; 10: 848–863.
22. MdIshak NA I, Kamarudin SK, Timmiati SN. Green synthesis of metal and metal oxide nanoparticles via plant extracts: an overview. *Mater Res Exp*. 2019; 6: 112004.
23. Jeevanandam J, Chan YS, Danquah MK. Biosynthesis of Metal and Metal Oxide Nanoparticles. *Chem Bio Eng Rev*. 2016; 3: 55–67.
24. Vijayakumar S, Mahadevan S, Arulmozhia P, Sriram S, Praseeth PK. Green synthesis of zinc oxide nanoparticles using *Atalantiamonophylla* leaf extracts: Characterization and antimicrobial analysis. *Mater Sci Sem Process*. 2018; 82: 39-45.
25. Hana S, Fuad A, Sami A, Abobakr A, Suaad A. *Padinaboryana* mediated green synthesis of crystalline palladium nanoparticles as potential nano drug against multidrug resistant bacteria and cancer cells. *Sci Rep*. 2021; 11: 5444.
26. Sana SS, Kumbhakar DV, Pasha A, Smita CP, Grace AN, Singh RP et al. *Crotalaria verrucosa* Leaf Extract Mediated Synthesis of Zinc Oxide Nanoparticles: Assessment of Antimicrobial and Anticancer Activity. *Molecules*. 2020; 25: 4896.
27. Jayachandran A, Aswathy TR, Nair AS. Green synthesis and characterization of zinc oxide nanoparticles using *Cayratiapedata* leaf extract. *Biochem Biophys Rep*. 2021; 26: 100995.
28. Makarov VV, Love AJ, Sinitsyna OV, Makarova SS, Yaminsky IV, Taliansky ME, et al. Green nanotechnologies: synthesis of metal nanoparticles using plants. *Acta Naturae*. 2014; 6 (1): 35–44.
29. Dhadapani P, Siddarth AS, Kamalasekaran S, Maruthamuthu S, Rajagopal G. Bio-approach: ureolytic bacteria mediated synthesis of ZnO nanocrystals on cotton fabric and evaluation of their antibacterial properties. *Carbo Polym*. 2014; 103: 448–455.

30. Shanthi S, Tharani SS. Green Synthesis of Zirconium Dioxide (ZrO<sub>2</sub>) Nano Particles Using *Acalypha Indica* Leaf Extract. *Int J Engi Applied Sci.* 2016; 3: 23-25.
31. Gowri S, Rajiv Gandhi R, Senthil S, Sundrarajan M. Effect of Calcination Temperature on *Nyctanthes Plant* Mediated Zirconia Nanoparticles; Optical and Antibacterial Activity for Optimized Zirconia. *J Bionano.* 2015; 9: 181–189.
32. Whangchai K, Shanmugam S, Van Le Q, Chau TP, Al-Kheraif AA, Brindhadevi K, et al. Study of antimicrobial activity of *Thespesiapopulnea*-coated nanozirconium on cotton gauze fabrics. *Appl Nano.* 2021. <https://doi.org/10.1007/s13204-021-01867-8>
33. Holišová V, cková ZK, Gabriela K, Kolenčík M, Niide T, Umetsu M, et al. Phytosynthesis of Au and Au/ZrO<sub>2</sub> bi-Phasic System Nanoparticles with Evaluation of Their Colloidal Stability. *J Nano Nanotech.* 2019; 19: 2807–2813.
34. Gowri S, Rajiv GR, Sundrarajan M. Structural, Optical, Antibacterial and Antifungal Properties of Zirconia Nanoparticles by Biobased Protocol. *J Mater Sci Technol.* 2014; 30(8): 782-790.
35. Goyal P, Bhardwaj A, Kumar Mehta B, Mehta D. Research article green synthesis of zirconium oxide nanoparticles (ZrO<sub>2</sub>NPs) using *Helianthus annuus* seed and their antimicrobial effects. *J Indian Chem Soc.* 2021; 98: 100089.
36. Annu A, Sivasankari C, Krupasankar U. Synthesis and characterization of ZrO<sub>2</sub> nanoparticle by leaf extract bioreduction process for its biological studies. *Mater Today: Proce.* 2020; 33: 5317-5323.
37. Isacfranklin M, Dawoud T, Ameen F, Ravi G, Yuvakkumar R, Kumar P, et al. Synthesis of highly active biocompatible ZrO<sub>2</sub>nanorods using a bioextract. *Ceramics Inter.* 2020; 46: 25915-25920.
38. Prasada KS, Amina Y, Selvaraj K. Defluoridation using biomimetically synthesized nano zirconium chitosan composite: Kinetic and equilibrium studies. *J Hazardous Mater.* 2014; 276: 232–240.
39. Felipe Viana da Silva A, Fagundes AP, Macuvelea DLP, Urano de Carvalho EF, Durazzo M, Padoina N, et al. Green synthesis of zirconia nanoparticles based on *Euclea natalensis* plant extract: Optimization of reaction conditions and evaluation of adsorptive properties. *Colloids Surf A.* 2019; 583: 123915.
40. Balaji S, Mandal BK, Ranjan S, Dasgupta N, Chidambaram R. Nano-zirconia – Evaluation of its antioxidant and anticancer activity. *J Photochem Photobio B.* 2017; 170: 125-133.
41. Gurushantha K, Anantharaju KS, Nagabhushana H, Sharma SC, Vidyad YS, Shivakumara C, et al. Facile green fabrication of iron-doped cubic ZrO<sub>2</sub> nanoparticles by *Phyllanthusacidus*: Structural, photocatalyticand photoluminescent properties. *J Mole Catalyst A.* 2015; 397: 36–47.
42. Shinde HM, Bhosale TT, Gavade NL, Babar SB, Kamble RJ, Shirke BS, et al. Biosynthesis of ZrO<sub>2</sub> nanoparticles from *Ficus benghalensis* leaf extract for photocatalytic activity. *J Mater Sci Mater Electron.* 2018; 29: 14055–14064.
43. Sai Saraswathi V, Santhakumar K. Photocatalytic activity against azo dye and cytotoxicity on MCF-7 cell lines of zirconium oxide nanoparticle mediated using leaves of *Lagerstroemia speciosa*. *J Photochem Photobio B.* 2017; 169: 47–55.
44. Nabil A, Muthuvel A, Jothibas M, Ali A, Fahad AA, Mohana V. Biosynthesis of zirconium oxide nanoparticles using *Wrightia tinctoria* leaf extract: Characterization, photocatalytic degradation and antibacterial activities. *Inorg Chem Comm.* 2021; 127: 108507.
45. Rasheed P, Haq S, Waseem M, Ur Rehman S, Wajid R, Bibi N, et al. Green Synthesis of Vanadium Oxide-Zirconium Oxide Nanocomposite for the Degradation of Methyl Orange and Picloram. *Mater Res Exp.* 2020; 7: 025011.
46. Alagarsamy A, Chandrasekaran S, Manikandan A. Green synthesis and characterization studies of biogenic zirconium oxide (ZrO<sub>2</sub>) nanoparticles for adsorptive removal of methylene blue dye. *J Mol Stru.* 2022; 1247: 131275.
47. Vennila R, Kamaraj P, Arthanareeswarid M, Sridharan M, Sudha G, Devikala S, et al. Biosynthesis of ZrO Nanoparticles And Its Natural Dye Sensitized Solar Cell Studies. *Mater Today: Proce.* 2018; 5: 8691–8698.
48. Renuka L, Anantharaju KS, Sharma SC, Nagaswarupa HP, Prashantha SC, Nagabhushana H et al. Hollow microspheres Mg-doped ZrO<sub>2</sub> nanoparticles: Green assisted synthesis and applications in photocatalysis and photoluminescence. *J Alloy Comp.* 2016; 672: 609-622.
49. Sathishkumar M, Sneha K, Yun Y-S. Green fabrication of zirconia nano-chains using novel *Curcuma longa* tuber extract. *Mater Lett.* 2013; 9: 242–245.
50. Davar F, Majedi A, Mirzaei A. Polyvinyl alcohol thin film reinforced by green synthesized zirconia nanoparticles. *Ceramics Inter.* 2018; 44: 19377–19382.
51. Nithya P, Balaji M, Jegatheeswaran S, Selvam S, Sundrarajan M. Facile biological synthetic strategy to morphologically aligned CeO<sub>2</sub>/ZrO<sub>2</sub> core nanoparticles using *Justiciaadhatoda* extract and ionic liquid: Enhancement of its bio-medical properties. *J Photochem Photo B.* 2018; 178: 481-488.
52. Raghad DHAJ, Maryam MHMJ, Abd AN. Plants extracts as green synthesis of zirconium oxide nanoparticles. *J Genetic Environ Res Conse.* 2017; 5(1): 6-23.
53. Krishnaraj C, Muthukumaran P, Ramachandran R, Balakumaran MD, Kalaichelvan PT. *Acalyphaindica* Linn: biogenic synthesis of silver and gold nanoparticles and their cytotoxic effects against MDA-MB-231, human breast cancer cells. *Biotechnol Rep.* 2014; 4: 42-49.
54. He S, Guo Z, Zhang Y, Zhang S, Wang J, Gu N. Biosynthesis of gold nanoparticles using the bacteria *Rhodopseudomonascapsulata*. *Mater Lett.* 2007; 6: 3984-3987.

55. Ahmad A, Mukherjee P, Senapati S, Mandal D, Khan MI, Kumar R et al. Extracellular Biosynthesis of silver nanoparticles using the fungus *Fusarium oxysporum*. *Colloids Surf B*. 2003; 28: 313-318.
56. Fayaz AM, Balaji K, Girilal M, Yadav R, Kalaichelvan PT, Venketesan R. Biogenic synthesis of silver nanoparticles and their synergistic effect with antibiotics: a study against gram-positive and gram-negative bacteria. *Nanomed Nanotechnol Biol Med*. 2010; 6: 103-109.
57. Debnath B, Majumdar M, Bhowmik M, Lal Bhowmik K, Debnath A, Roy DN. The effective adsorption of tetracycline onto zirconia nanoparticle synthesized by novel microbial green technology. *J Environ Manag*. 2020; 261: 110235.
58. Ahmed T, Ren H, Noman M, Shahid M, Liu M, AliMd A, et al. Green synthesis and characterization of zirconium oxide nanoparticles by using a native *Enterobacter* sp. and its antifungal activity against bayberry twig blight disease pathogen *Pestalotiopsis versicolor*. *NanoImpact*. 2021; 21: 100281.
59. Suriyaraj S P, Ramadoss G, Chandraraj K, Selvakumar R. One pot facile green synthesis of crystalline bio-ZrO<sub>2</sub> nanoparticles using *Acinetobacter* sp. KCS11 under room temperature. *Mater Sci Eng C*. 2019; 105: 110021.
60. Zielonka A, Klimek-ochab M. Fungal synthesis of size-defined nanoparticles Related content. *Adv Nat Sci Nanosci Nanotechnol*. 2017; 8: 1-9.
61. Al-Enazi NM, Ameen F, Alsamhary K, Dawoud T, Al-Khattaf F, AlNadhari S. Tin oxide nanoparticles (SnO<sub>2</sub>-NPs) synthesis using *Galaxaura elongate* and its antimicrobial and cytotoxicity study: a greenery approach. *Appl Nano*. 2021. <https://doi.org/10.1007/s13204-021-01828-1>
62. Jain N, Bhargava A, Majumdar S, Tarafdar JC, Panwar J. Extracellular Biosynthesis and characterization of silver nanoparticles using *Aspergillus flavus* NJP08: a mechanism prospective. *Nanoscale*. 2011; 3 (2): 635-641.
63. Ghomi A RG, Mohammadi-Khanaposhti M, Vahidi H, Kobarfard F, Ameri Shah Reza M, et al. Fungus-mediated Extracellular Biosynthesis and Characterization of Zirconium Nanoparticles Using Standard *Penicillium* Species and Their Preliminary Bactericidal Potential: A Novel Biological Approach to Nanoparticle Synthesis. *Iran J Pharma Res*. 2019; 18 (4): 2101-2110.
64. Golnaraghi-Ghomi AR, Mohammadi-Khanaposhti M, Sokhansanj A, Saadati Y, Khazraei E, Kobarfard F, et al. Artificial Neural Network Modeling of Fungus-Mediated Extracellular Biosynthesis of Zirconium Nanoparticles Using Standard *Penicillium* spp. *J Cluster Sci*. 2021; 1-15.
65. Kavitha NS, Venkatesh KS, Palani NS, Ilangoan R. Synthesis and characterization of zirconium oxide nanoparticles using *Fusarium solani* extract. *AIP Conf Pro*. 2020; 2265: 030057.
66. Bansal V, Rautaray D, Ahmad A, Sastry M. Biosynthesis of zirconia nanoparticles using the fungus *Fusarium oxysporum*. *J Mater Chem*. 2004; 14:3303-3305.
67. Uddin I, Ahmad A. Bioinspired eco-friendly synthesis of ZrO<sub>2</sub> nanoparticles. *J Mater Environ Sci*. 2016; 7 (9): 3068-3075.
68. Mukherjee P, Roy M, Mandal B, Dey G, Mukherjee P, Ghatak J, et al. Green synthesis of highly stabilized nanocrystalline silver particles by a non-pathogenic and agriculturally important fungus *Trichodermaasperellum*. *Nanotech*. 2008; 19: 75103-75110.
69. Dahoumane SA, Yepremian C, Djediat C, Coute A, Fievet F, Coradin T, et al. A global approach of the mechanism involved in the Biosynthesis of gold colloids using micro-algae. *J Nanoparticle Res*. 2014; 16: 2607.
70. Kumaresan M, VijaiAnand K, Govindaraju K, Tamilselvan S, Ganesh Kumar V. Seaweed *Sargassum wightii* mediated preparation of zirconia (ZrO<sub>2</sub>) nanoparticles and their antibacterial activity against gram-positive and gram-negative bacteria. *Micro Pathoge*. 2018; 124: 311-315.



## التطورات الحديثة في التخليق الحيوي لجسيمات أكسيد الزركونيوم النانوية وتطبيقاتها البيولوجية

محمد سليمان<sup>4</sup>

منى الطامي<sup>3</sup>

منيفة العنزي<sup>2</sup>

سلام الشراري<sup>1</sup>

- <sup>1</sup> قسم الأحياء، كلية العلوم، جامعة الجوف ص.ب. ب 72341، سكاكا، المملكة العربية السعودية
- <sup>2</sup> قسم الأحياء، كلية العلوم، جامعة تبوك، تبوك، المملكة العربية السعودية
- <sup>3</sup> قسم الأحياء، كلية العلوم، جامعة القصيم، بريدة، المملكة العربية السعودية
- <sup>4</sup> الخطة الوطنية للعلوم والتكنولوجيا والابتكار، جامعة الملك سعود، الرياض، المملكة العربية السعودية

### الخلاصة:

أثار أكسيد الزركونيوم  $ZrO_2$  اهتمام الباحثين في جميع أنحاء العالم، لا سيما منذ تطوير طرق لتصنيع جزيئات بحجم النانو. تم تحفيز الدراسة المكثفة في تكوين الجسيمات النانوية باستخدام تقنيات تركيبية مختلفة، بالإضافة إلى استخداماتها المحتملة، من خلال كفاءتها الضوئية العالية، وفجوة النطاق العريض، وطاقة ربط الأكسيتون العالية في تغليف المواد الغذائية، يمكن استخدام الجسيمات النانوية لثاني أكسيد الزركونيوم كعوامل مضادة للميكروبات ومضادة للسرطان. استجابةً للاهتمام المتزايد بـ  $nano ZrO_2$ ، ابتكر الباحثون وطوروا طرقاً لتكوين الجسيمات النانوية. تم مؤخراً إنشاء مركبات  $ZrO_2$  النانوية ذات الأشكال المختلفة باستخدام طرق بيولوجية ("الكيمياء الخضراء"). تساهم كل من الميكروبات والنباتات في إنتاج الزركونيا في المختبر. يتم توفير عوامل التثبيت بواسطة الجزيئات الحيوية الموجودة في المستخلصات النباتية، بينما يتم توفير الإنزيمات بواسطة الكائنات الحية الدقيقة كعوامل للتغطية والتثبيت (داخل الخلايا أو خارج الخلية). من الممكن تحليل الجسيمات النانوية المنتجة باستخدام مجموعة متنوعة من الأساليب التحليلية، بما في ذلك التحليل الطيفي للأشعة فوق البنفسجية المرئية، وحيود الأشعة السينية (XRD)، والمجهر الإلكتروني للإرسال (TEM)، والتحليل الطيفي للأشعة تحت الحمراء (FT-IR). عند تطبيقها على البكتيريا (موجبة الجرام وسالبة الجرام) والفطريات، تظهر  $ZrO_2$ NPs قدرات واعدة مضادة للجراثيم. تعتبر الخلايا الطبيعية والخبيثة حساسة للجسيمات النانوية  $ZrO_2$ ، والتي يمكن تفسيرها من خلال توليد الأكسجين التفاعلي (ROS). يناقش هذا العمل ويصف الطرق العديدة لإنتاج جسيمات  $ZrO_2$  النانوية، بالإضافة إلى خصائصها وإمكانات التطبيق المختلفة.

**الكلمات المفتاحية:** التطبيقات، الخصائص، التخليق الأخضر، النانو تكنولوجي، جزيئات الزركونيوم النانوية